A Multifunctional Microwave Filter/Sensor Component Using a Split Ring Resonator Loaded Transmission Line

Zahra Shaterian , *Member, IEEE*, and Michal Mrozowski , *Fellow, IEEE*

Abstract—This research is focused on the design and realization of a microwave component with multifunctional filter/sensor operation using a resonator-loaded transmission line (TL). It is shown that while the structure acts as a bandstop filter, the phase of the reflection coefficient from the loading resonator(s) on a movable layer can be used for displacement sensing, thus allowing for combining filtering with sensing in one device. The proposed multifunctional mechanism is validated through electromagnetic (EM) simulation of the structure. The concept and the performance of the proposed device are further examined through the fabrication and measurement of a multifunctional filter/sensor component based on a microstrip TL loaded with movable split ring resonators (SRRs).

Index Terms—Filter, microwave displacement sensor, multifunctional component, phase, split ring resonator (SRR).

I. Introduction

IN RESPONSE to increasing demand for portable wireless communication devices, many studies have been focused on the development of compact, lightweight, and low-cost microwave components. One popular method to achieve these goals is by integrating components with different functionality to form multifunctional components. Filters are one of the widely used passive components that are present in the radio frequency (RF) front-end of almost any wireless communication system. Filters operating at high microwave and millimeter-wave frequencies are realized using distributed elements, thus consuming a relatively large area. That is why many studies have been conducted to integrate microwave filters with other components to form multifunctional components, thus reducing the overall size and weight. Filtering antennas [1], filtering power dividers [2], and filtering power amplifiers [3] are some examples of such multifunctional components.

Microwave sensors are another category of microwave components that are widely used for different applications such as
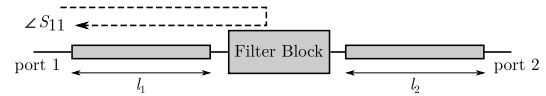
Fig. 1. Block diagram for the proposed multifunctional filter/sensor component.

material characterization [4], [5], defect detection [6], [7], [8], rotation [9], [10], [11], [12], and displacement sensing [13], [14], [15]. The functionality of all the above-mentioned structures is limited only to sensing. However, the availability of new RF circuits that can simultaneously provide typical RF signal processing actions such as filtering, and RF/microwave sensing can be very advantageous, especially for the Internet of Things (IoT) devices. Despite their extensive applications, studies on the integration of microwave sensors with other passive or active components are very limited. To the best of the authors' knowledge, the first multifunctional filter/sensor has very recently been proposed in [16]. The frequency response of the ultra-wideband (UWB) filter in [16] possesses a transmission zero, which is located in the passband region. The frequency of the transmission zero is sensitive to the angular displacement of a rotatable section. Therefore, the sensing is performed by monitoring a shift in the frequency of the transmission zero. Despite the proper operation of this sensor in the UWB filter, this method is not applicable for integrating a sensor with narrowband filters.

This letter presents a novel method for the design of multifunctional filter/sensor components. In this method, sensing is conducted based on the variations of the phase while the magnitude response, which is the one that matters in most filters, is used for filtering operation. For demonstration, a multifunctional component that provides a bandstop filtering response while sensing a linear displacement is presented.

II. Principle of Operation and Numerical Validation

Fig. 1 illustrates a block diagram for the proposed multifunctional filter/sensor component. As shown in the figure, the structure is composed of a bandstop filter block, which is sandwiched between two 50 Ω transmission line (TL) sections. In this configuration, a signal fed at one port reaches the other port at all frequencies except in the stopband of the filter where the signal will be reflected back to the source. Note that the phases of the reflection coefficients, i.e., $\angle S_{11}$ and $\angle S_{22}$ change if the lengths l_1 and l_2 are altered. Therefore, variations in the phase of reflection coefficients due to changes in the lengths l_1 and/or l_2 or their propagation constants can be used for
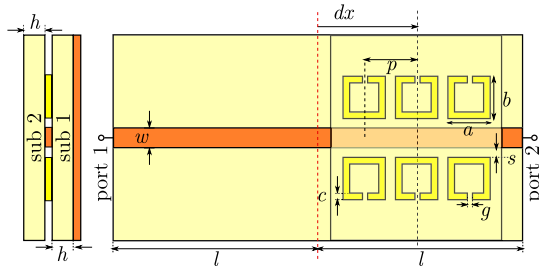
Fig. 2. Side and top views of the proposed structure for multifunctional filter/sensor. The microstrip line has a width of $w = 1.15$ mm, which corresponds to a 50-Ω characteristic impedance. The dimensions of the first and third resonators are: $a = 4.8$ mm, $b = 4.8$ mm, $g = 0.3$ mm, $c = 0.3$ mm, and the spacing s between each SRR and the microstrip is 0.2 mm. Dimensions of the second pair of SRRs are $b_2 = 4.82$ mm and $s_2 = 0.16$ mm. The space between two adjacent SRRs is $p = 7.4$ mm.
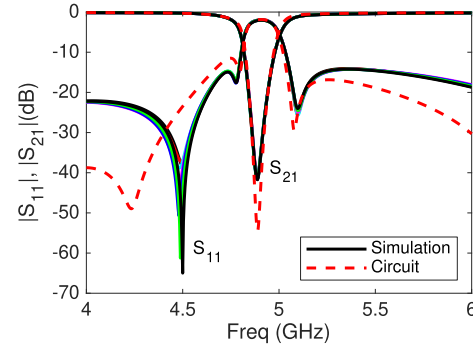

Fig. 3. Circuit and EM simulated magnitude of the transmission and reflection coefficients of the proposed component for different values of displacement.

sensory applications. It is very important to note that if small losses are neglected, the magnitude of the transmission and reflection coefficients, i.e., $|S_{21}|$ and $|S_{11}|$ are independent of the TL lengths l_1 and l_2. Therefore, changes in the lengths l_1 and/or l_2 do not have any effect on the magnitude response, which is the one that matters in most filters. In short, using this method, simultaneous sensing and filtering functionalities are achieved while avoiding undesired mutual effects. Note that the filter block in Fig. 1 can be either a simple notch filter formed by a single loading resonator or an elaborate high-order Butterworth or Chebyshev bandstop filter.

For demonstration, in what follows, a multifunctional third-order Chebyshev bandstop filter and displacement sensor is presented. The TLs are realized in microstrip technology while split ring resonators (SRRs) are utilized as the main building blocks of the filter. Fig. 2 shows the proposed filter/sensor structure. As shown in the figure, the structure is composed of two substrates that are stacked on top of each other. A microstrip line and its ground plane are implemented on the top and bottom layers of the first substrate, while three pairs of SRRs are realized on the second substrate.

At the initial position when the SRRs are symmetrically placed with respect to the input and output ports of the TL, i.e., $dx = 0$, the phase of the reflected signal by the SRRs is $\angle S_{11} = -2\beta l$, where l is the half length of the microstrip line, and β is the phase constant of the TL. Displacing the top substrate in the longitudinal direction by dx changes the position of SRRs along the TL. This in turn increases the traveling path of a signal from port 1 to the SRRs to $l + dx$. As a result, the phase of the reflected signal by the SRRs to port 1 will be $-2\beta(l + dx)$. Thus, a displacement in the x-direction can be accurately determined by measuring the phase of the reflected signal. As mentioned earlier, displacement of the SRRs only changes the phase of the reflected signals, while the magnitudes of the transmitted and reflected signals and as a result, the filtering behavior of the component is untouched.

To validate the concept, a narrowband Chebyshev bandstop filter with the center frequency $f_0 = 4.9$ GHz, 5.3% fractional bandwidth (FBW), and 0.1 dB insertion loss in the passband is designed and simulated. The filter design is started with the element values of the corresponding lowpass prototype, i.e., $g_0 = g_4 = 1.0$, $g_1 = g_3 = 1.0316$, and $g_2 = 1.1474$. The elements for the LC resonators transformed to the bandstop

filter are

$$C_p = \left(\frac{1}{\text{FBW}\omega_0\Omega_c}\right)\frac{1}{\gamma_0 g} \quad (1)$$

$$L_p = \left(\frac{\Omega_c\text{FBW}}{\omega_0}\right)\gamma_0 g \quad (2)$$

where γ_0 is the impedance scaling factor and Ω_c is the lowpass cutoff frequency. Using the above equations the required equivalent capacitance and inductance values for each pair of SRRs are as follows: $C_1 = C_3 = 11.916$ pF, $C_2 = 10.7$ pF, $L_1 = L_3 = 0.089$ nH, and $L_2 = 0.099$ nH. Then the geometric dimensions of each pair of SRRs should be optimized to meet these values and also achieve the resonance at the central frequency of the filter [17], [18], [19]. Note that the equivalent capacitance of a pair of SRRs can be obtained using the susceptance slope of the resonator from electromagnetic (EM) simulations using

$$C = \frac{1}{2}\frac{dB}{d\omega}\bigg|_{\omega=\omega_0}. \quad (3)$$

Rogers $RO4350$ material with a relative permittivity $\epsilon_r = 3.46$ and dielectric loss tangent $\tan(\delta) = 0.004$, thickness $h = 0.508$ mm, and 35 μm thick copper metallization is used for both substrates. Other dimensions of the structure are as denoted in the caption of Fig. 2. The dimensions of the second pair of SRRs are slightly different from the other pair of SRRs. Note that, conventionally all the resonators of a filter are chosen to be identical and the required equivalent capacitance and inductance values are achieved by utilizing different impedance inverter values K between the resonators. However, since in our design the SRRs are movable, the microstrip line has to be uniform. That is, no variations in K-values are allowed. Therefore, the dimensions of SRRs are adjusted to achieve the C_p, and L_p that are calculated based on (1) and (2).

For validation, the designed multifunctional filter/sensor is numerically simulated using HFSS full-wave EM simulation software. Fig. 3 depicts the circuit and the full-wave EM simulated magnitude of the transmission and reflection coefficients of the proposed multifunctional filter/sensor for different values of displacement dx from -6 to 6 mm in steps of 2 mm. Also, the simulated phase of reflection coefficient at port 1 (i.e., $\angle S_{11}$) versus frequency for different values of displacement from -6 to 6 mm in steps of 2 mm is presented in Fig. 4. As can be seen in Fig. 3, the signal entering port 1
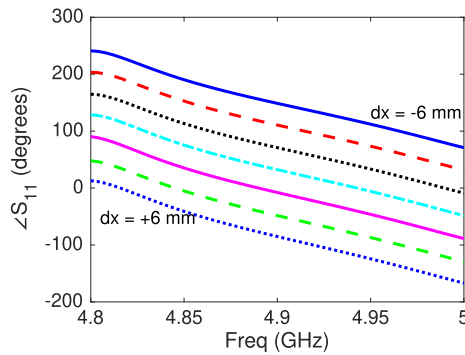
Fig. 4. Simulated phase of the reflection coefficient for different values of displacement dx from -6 to 6 mm in steps of 2 mm.

Fig. 7. Simulated and measured phase of the reflection coefficient versus displacement dx at $f = 4.8$, 4.9, and 5 GHz. Each value in the measured phase is the mean of five independent measurements for each setting of displacement and error bars represent the standard error of the mean.
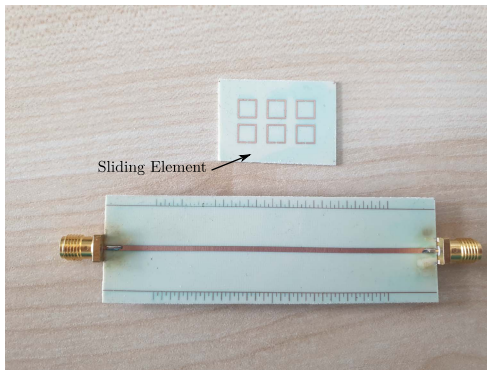

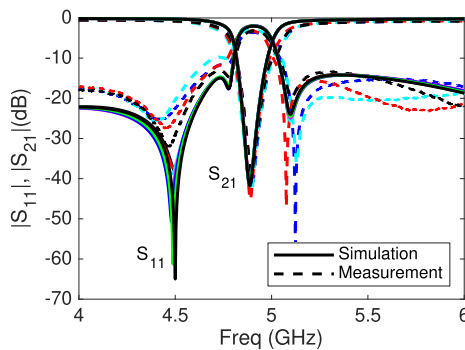Fig. 5. Photograph of the fabricated prototype.

Fig. 6. Measured (dashed line) and simulated (solid line) amplitude of the transmission and reflection coefficients for different values of displacement.

reaches port 2 at all frequencies except in the stopband of the filter (centered at $f = 4.9$ GHz). Note that displacing the top layer changes neither the amplitude nor the frequency of the transmission and the reflection coefficients. However, Fig. 4 shows that the phase of the reflection coefficient is a function of displacement dx. Therefore, the simulation results show that the amount of displacement can be sensed by measuring the phase of the reflected wave without any adverse effects on the amplitude of S-parameters for filtering functionality.

III. EXPERIMENTAL RESULTS

To validate the simulation results, the designed filter/displacement-sensor has been fabricated and its performance is measured. Fig. 5 shows the photograph of the fabricated prototype. The dimensions of the fabricated prototype correspond to the simulated structure in Section II. Measured and simulated amplitude of the transmission and reflection
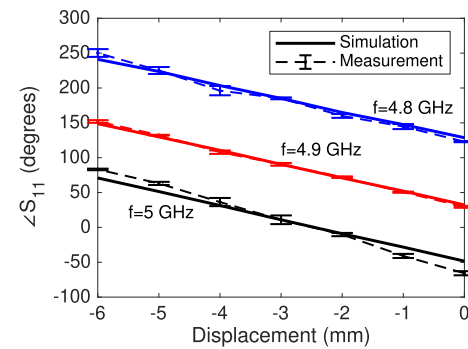
coefficients for different values of displacement dx from -6 to 0 mm by steps of 2 mm are shown in Fig. 6. The small discrepancy between the simulated and measured results may be attributed to the conductor loss, losses of the subminiature version A (SMA) connectors, fabrication tolerances, and small misalignment of the SRRs with respect to the symmetry plane of the loaded TL. The simulated and measured phase of the reflection coefficient at port 1 versus displacement dx at the center frequency of the filter, i.e., $f = 4.9$ GHz, is depicted in Fig. 7. It can be seen from this figure that by increasing dx the phase of S_{11} at $f = 4.9$ GHz is decreased, while the magnitude of the reflection and transmission coefficients (shown in Fig. 6) is almost unaffected. Fig. 7 also shows the simulated and measured phase of S_{11} versus displacement for $f = 4.8$ and 5 GHz. The presented results show that the sensor properly operates over the frequency band of the filter. Note that the phase of the S_{11} in the band stop of the filter, i.e., at the frequency band in which the amplitude of the S_{11} is close to 0 dB, is used for sensing application. Fig. 7 also shows that the measured and simulation results are in good agreement. Note that the proposed sensor benefits from a linear response with a high sensitivity of 20°/mm. Since the operating frequency of the sensor is dictated by the filter, the sensitivity of the sensor cannot be improved by increasing the operating frequency of the sensor. However, this aim can be met by the phase constant of the SRR-loaded TL. This is possible by using a substrate with a higher permittivity and/or thickness. It is worth mentioning that theoretically, the dynamic range of the sensor is infinite. However, in practice, the dynamic range is limited to the length of the microstrip line sections.

IV. CONCLUSION

A novel method for the design of a multifunctional microwave filter/sensor has been proposed. It has been shown that in bandstop filters where only the amplitude response matters, the phase of the reflected signal can be used for sensing purposes, with no adverse effect on filtering behavior. For demonstration, a third-order Chebyshev bandstop filter/sensor in microstrip technology has been designed. A prototype of the designed multifunctional device has been fabricated and its performance has been measured. The proposed concept has been validated by the good agreement between the EM simulated and experimentally measured results.

REFERENCES

[1] P. P. Shome, T. Khan, S. K. Koul, and Y. M. M. Antar, "Filtenna designs for radio-frequency front-end systems: A structural-oriented review," *IEEE Antennas Propag. Mag.*, vol. 63, no. 5, pp. 72–84, Oct. 2020.

[2] R. Gómez-García, R. Loeches-Sánchez, D. Psychogiou, and D. Peroulis, "Single/multi-band Wilkinson-type power dividers with embedded transversal filtering sections and application to channelized filters," *IEEE Trans. Circuits Syst. I, Reg. Papers*, vol. 62, no. 6, pp. 1518–1527, Jun. 2015.

[3] Y. C. Li, K. C. Wu, and Q. Xue, "Power amplifier integrated with bandpass filter for long term evolution application," *IEEE Microw. Wireless Compon. Lett.*, vol. 23, no. 8, pp. 424–426, Aug. 2013.

[4] C.-L. Yang, C.-S. Lee, K.-W. Chen, and K.-Z. Chen, "Noncontact measurement of complex permittivity and thickness by using planar resonators," *IEEE Trans. Microw. Theory Techn.*, vol. 64, no. 1, pp. 247–257, Jan. 2016.

[5] L. Su, J. Munoz-Enano, P. Velez, M. Gil-Barba, P. Casacuberta, and F. Martin, "Highly sensitive reflective-mode phase-variation permittivity sensor based on a coplanar waveguide terminated with an open complementary split ring resonator (OCSRR)," *IEEE Access*, vol. 9, pp. 27928–27944, 2021.

[6] S. Kharkovsky, A. McClanahan, R. Zoughi, and D. D. Palmer, "Microwave dielectric-loaded rectangular waveguide resonator for depth evaluation of shallow flaws in metals," *IEEE Trans. Instrum. Meas.*, vol. 60, no. 12, pp. 3923–3930, Dec. 2011.

[7] A. M. Albishi, M. S. Boybay, and O. M. Ramahi, "Complementary split-ring resonator for crack detection in metallic surfaces," *IEEE Microw. Wireless Compon. Lett.*, vol. 22, no. 6, pp. 330–332, Jun. 2012.

[8] S. Deif and M. Daneshmand, "Long array of microwave sensors for real-time coating defect detection," *IEEE Trans. Microw. Theory Techn.*, vol. 68, no. 7, pp. 2856–2866, Jul. 2020.

[9] A. Ebrahimi, W. Withayachumnankul, S. F. Al-Sarawi, and D. Abbott, "Metamaterial-inspired rotation sensor with wide dynamic range," *IEEE Sensors J.*, vol. 14, no. 8, pp. 2609–2614, Aug. 2014.

[10] Z. Shaterian, A. K. Horestani, and C. Fumeaux, "Rotation sensing based on the symmetry properties of an open-ended microstrip line loaded with a split ring resonator," in *Proc. German Microw. Conf.*, Mar. 2015, pp. 33–35.

[11] A. H. Karami, F. K. Horestani, M. Kolahdouz, A. K. Horestani, and F. Martín, "2D rotary sensor based on magnetic composite of microrods," *J. Mater. Sci., Mater. Electron.*, vol. 31, no. 1, pp. 167–174, Dec. 2020.

[12] A. K. Jha, A. Lamecki, M. Mrozowski, and M. Bozzi, "A microwave sensor with operating band selection to detect rotation and proximity in the rapid prototyping industry," *IEEE Trans. Ind. Electron.*, vol. 68, no. 1, pp. 683–693, Jan. 2021.

[13] J. Naqui and F. Martín, "Transmission lines loaded with bisymmetric resonators and their application to angular displacement and velocity sensors," *IEEE Trans. Microw. Theory Techn.*, vol. 61, no. 12, pp. 4700–4713, Dec. 2013.

[14] A. K. Horestani, Z. Shaterian, D. Abbott, and C. Fumeaux, "Application of metamaterial-inspired resonators in compact microwave displacement sensors," in *Proc. 1st Austral. Microw. Symp. (AMS)*, Jun. 2014, pp. 19–20.

[15] Z. Mehrjoo, A. Ebrahimi, and K. Ghorbani, "Microwave resonance-based reflective mode displacement sensor with wide dynamic range," *IEEE Trans. Instrum. Meas.*, vol. 71, pp. 1–9, 2022.

[16] C.-H. Chio, K.-W. Tam, and R. Gomez-Garcia, "Filtering angular displacement sensor based on transversal section with parallel-coupled-line path and U-shaped coupled slotline," *IEEE Sensors J.*, vol. 22, no. 2, pp. 1218–1226, Jan. 2021.

[17] J. D. Baena *et al.*, "Equivalent-circuit models for split-ring resonators and complementary split-ring resonators coupled to planar transmission lines," *IEEE Trans. Microw. Theory Techn.*, vol. 53, no. 4, pp. 1451–1461, Apr. 2005.

[18] A. K. Horestani, C. Fumeaux, S. F. Al-Sarawi, and D. Abbott, "Split ring resonators with tapered strip width for wider bandwidth and enhanced resonance," *IEEE Microw. Wireless Compon. Lett.*, vol. 22, no. 9, pp. 450–452, Sep. 2012.

[19] H.-X. Xu, G.-M. Wang, Z.-M. Xu, X. Chen, Z. Yu, and L. Geng, "Dual-shunt branch circuit and harmonic suppressed device application," *Appl. Phys. A, Solids Surf.*, vol. 108, no. 2, pp. 497–502, Apr. 2012.